International Journal for Computational Civil and Structural Engineering, 22(2) 206–229 (2026)

DOI:10.22337/2587-9618-2026-22-2-206-229

NUMERICAL PARAMETRIC ANALYSIS OF AXIALLY COMPRESSED CIRCULAR STEEL TUBE CONFINED CONCRETE COLUMNS

Vladislav V. Vershinin

National Research Moscow State University of Civil Engineering, Moscow, RUSSIA

Abstract: Axially compressed circular steel tube confined concrete columns have been parametrically analyzed through numerical simulation with the general aim to confirm the effectiveness of concrete confinement and quantitatively estimate it. Numerical models have been assembled using SIMULIA Abaqus finite element analysis commercial software and its relevant tools, in particular Abaqus/Explicit module, the general contact algorithm, and the concrete damaged plasticity model. The limit states of the first group and corresponding failure mechanisms have been defined for the considered columns and investigated, qualitatively and quantitatively, with regard to their dependence onto column structural scheme, steel tube thickness and concrete grade. Totally, 33 different cases have been simulated and analyzed.

Keywords: steel tube confined concrete column, numerical simulation, parametrical analysis, concrete damaged plasticity model

ЧИСЛЕННЫЙ ПАРАМЕТРИЧЕСКИЙ АНАЛИЗ ЦЕНТРАЛЬНО СЖАТЫХ ТРУБОБЕТОННЫХ КОЛОНН

В.В. Вершинин

Национальный исследовательский Московский государственный строительный университет, г. Москва, РОССИЯ

Аннотация: Выполняется численный параметрический анализ центрально сжатых трубобетонных колонн с целью подтвердить положительное влияние стеснения поперечных деформаций бетона на несущую способность конструктивного элемента и количественно оценить его эффект. Построение численных моделей выполняется в коммерческом программном комплексе конечно-элементного анализа SIMULIA Abaqus с использованием соответствующих инструментов, в частности модуля Abaqus/Explicit, универсального метода решения контактных задач и математической модели неупругого поведения бетона. Определяются предельные состояния первой группы и соответствующие им механизмы разрушения конструктивного элемента. Проводится качественный и количественный анализ зависимости значений их параметров от расчётной схемы колонны, толщины стальной трубы и класса бетона по прочности на одноосное сжатие. Всего рассматриваются 33 различных случая.

Ключевые слова: трубобетонная колонна, численное моделирование, параметрический анализ, математическая модель неупругого поведения бетона

1. INTRODUCTION

Concrete, similarly to many other materials, exhibits pronounced dependence of its strength onto a stress state. For instance, according to Russian building code SP 63.13330.2018 “Concrete and reinforced concrete structures. General provisions” [1], the ratio of normal-weight concrete strength under uniaxial compression to its strength under uniaxial tension varies from 7.6 for grade B5 concrete to 21.6 for grade B100 concrete, exhibiting non-linear, viz. power, increase with concrete grade. Typical experimental values of the ratio of concrete strength under biaxial compression to its strength under uniaxial compression are in the range from 1.10 to 1.16 [2]. These concrete strength properties were reflected into elaborate strength criteria, developed in 1970s specifically to describe concrete inelastic behaviour [3-6].

Concrete, being relatively inexpensive and available almost everywhere, is one of the most widely used construction materials. In construction, its strength properties described above are utilized in conjunction with various structural measures. The most common way is using reinforced concrete instead of plain one, so that tensile stresses in structural elements are taken up by the reinforcement, while concrete withstands to compressive stresses. Yet, commonly employed structural measures do not completely exploit concrete high compressive strength, especially under complex stress states.

While most vertical structural elements (columns, shear walls and composite elements) experience complex loading – axial compression, shear in horizontal direction, bending about a horizontal axis, and torsion around the vertical axis, – compressive stresses are predominant in most cases, except, probably, an earthquake excitation, when horizontal inertia forces can result in shear stresses of the same order of magnitude as the compressive stresses. The corresponding stress state can be characterized as close to the uniaxial one. And only for structures with large length-to-width ratio the stress state is close to the plane strain compression. Yet, concrete strength under biaxial compression, plane strain compression, and all-around compression is significantly higher than that under uniaxial compression. Hence, there is an evident profit from changing the stress state of a structural element from a uniaxial one to some more complex through some structural measures. An effective measure is to restrict lateral straining of vertical structural elements, so that their response becomes close to uniaxial straining and, hence, triaxial compression. A common way to provide concrete confinement is to use a steel tube. Such a structural solution is called “steel tube confined concrete” and is commonly employed for columns, especially for heavily loaded ones.

The steel tube confined concrete columns, despite working mainly under uniaxial compression, exhibit rather complex behaviour. Complex response of such columns is caused by several factors.

First of all, it is a structural scheme of the considered element. Some structural solutions provide loads acting onto ends of both steel and concrete parts of the column, while in other cases only a concrete core is loaded, and steel tube acts only as a confinement. Evidently, this yields two different schemes of interaction between the steel tube and the concrete core.

Secondly, Young’s moduli of steel and concrete differ from each other by almost an order of magnitude, and values of their Poisson’s ratios differ by 50%. Moreover, not only concrete compressive-to-tensile strength ratio increases with grade, so does its Young’s modulus.

In the third place, construction steel is a highly plastic material, whose strains at failure exceed unity under some stress states, while concrete is a quasi-brittle material, which, being inelastically deformed, experiences either cracking (under tension) or crushing and pronounced dilation (under compression or shear).

Finally, the level of strains under which concrete loses almost all of its bearing capacity (approximately 0.003-0.004) corresponds to the very beginning of a plastic phase of straining for construction steel, which retains its strength and stiffness well beyond this level of plastic straining.

In the present work, axially compressed circular steel tube confined concrete columns have been parametrically analyzed through numerical simulation. The first group of column limit states and corresponding column failure mechanisms have been investigated, qualitatively and quantitatively, with regard to their dependence onto column structural scheme, steel tube thickness and concrete grade.

2. PROBLEM FORMULATION

The steel tube confined concrete column with a circular cross-section subjected to an axial compressive load has been considered. The reference cross-section diameter has been chosen

to be equal to 720 mm. The column height has been set equal to 3 m.

Axial loading of the column has been performed through two rigid dies. The bottom die has been fixed, and the top die has been able to move only in vertical direction.

The top die has been loaded through the Kelvin-Voigt viscoelastic element, that has allowed one to obtain decreasing parts of a "force-displacement" curve and damp out oscillations in the curve, which have appeared due to concrete cracking and crushing. This Kelvin-Voigt viscoelastic element has been assumed to simulate the actuator of the test machine and have the following properties: the elastic stiffness $K = 1.0 \cdot 10^9$ N/m, and the damping factor $C = 1.0 \cdot 10^4$ N·s/m.

For each die an artificial associated mass has been specified in the form of a point mass located at its center and having the following properties: 20 kg for translational degrees of freedom and $0.02\ \text{kg} \cdot \text{m}^2$. A point mass with the same properties has been specified for the free end of the Kelvin-Voigt viscoelastic element.

Loading of the column has been carried out through assigning a constant velocity of 0.4 m/s in the vertical direction to the free end of the Kelvin-Voigt viscoelastic element.

At the contact interfaces between the dies and the column ends, the isotropic Coulomb friction has been assumed to take place with the friction factor μ being equal to 0.2 for the contact interfaces between the dies and the steel tube ends, and 0.35 for the contact interfaces between the dies and the concrete core ends.

The isotropic Coulomb friction has been assumed to take place at the contact interface between the concrete core and the steel tube as well. The friction factor μ has been assumed to be equal to 0.35 at this contact interface.

Since the parametrical analysis has been performed, a four index notation of the form

$$A\text{-}B\text{-}C\text{-}D \qquad (1)$$

has been established to distinguish particular cases.

The first index, *A*, specifies the column structural scheme. It equals to 1 in the case, when the axial load acts onto ends of both steel and concrete parts of the column, and equals to 2 in the case, when only the concrete core is subjected to axial loading, while the steel tube acts only as a confinement.

The second index, *B*, specifies the concrete grade. Totally, three normal weight concrete grades have been considered – B30, B60, and B90, – with index *B* taking these particular values. Also a reference case with no concrete core, but only steel tube has been considered to be able to determine what fraction of a column load-bearing capacity is provided by the steel tube. In this case, index *B* equals to zero.

The third index, *C*, specifies the steel tube thickness. Totally, three different steel tube thickness values have been considered, – 10 mm, 20 mm, and 30 mm, – with index *C* taking these particular values. Also a reference case with no steel tube, but plain concrete column has been considered to quantitatively determine the effectiveness of concrete confinement. In this case, index *C* equals to zero.

The fourth index, *D*, specifies the concrete core diameter. According to the index *C* possible values, the corresponding values of index *D* are 720, 700, 680, and 660.

All in all, 33 different cases have been simulated and analyzed: 1-0-10-0, 1-B30-10-700, 1-B60-10-700, 1-B90-10-700, 1-0-20-0, 1-B30-20-680, 1-B60-20-680, 1-B90-20-680, 1-0-30-0, 1-B30-30-660, 1-B60-30-660, 1-B90-30-660, 2-B30-0-720, 2-B60-0-720, 2-B90-0-720, 2-B30-0-700, 2-B60-0-700, 2-B90-0-700, 2-B30-0-680, 2-B60-0-680, 2-B90-0-680, 2-B30-0-660, 2-B60-0-660, 2-B90-0-660, 2-B30-10-700, 2-B60-10-700, 2-B90-10-700, 2-B30-20-680, 2-B60-20-680, 2-B90-20-680, 2-B30-30-660, 2-B60-30-660, 2-B90-30-660.

In all the relevant cases, the ends of the concrete core have been reinforced with a single rebar mat. It has been assumed, that these mats have had a 100×100 mm grid and have been made of

class A500C (according to Russian standards) steel rods with the diameter of 6 mm. In the cases, when the concrete core has been confined by the steel tube, these rebar mats have been welded to the tube.

The steel tube has been assumed to be made of class C355 (according to Russian standards) steel in all the relevant cases.

3. NUMERICAL MODELS

Numerical models of the considered steel tube confined concrete column have been assembled and analyzed using SIMULIA Abaqus finite element analysis commercial software. Some of them are presented in Fig. 1.

The considered problem has been solved quasi-statically, with geometrical nonlinearity taken into account, using Abaqus/Explicit module, in which the central difference time integration scheme of the second order of accuracy is implemented. To fulfil the Courant-Friedrichs-Lewy stability condition, a stable time increment has been automatically determined by the solver itself during the solution. (An interested reader is referred to software documentation [7, 8] for more details.)

At each contact interface a contact problem, with all the features described above in Section 2, has been solved through a General Contact algorithm implemented into Abaqus/Explicit, within which contact constraints are enforced through a penalty contact algorithm. The surfaces of the concrete core and the steel tube at their contact interface have been smoothed using a Surface Smoothing tool to preclude artificial contact stress oscillations and high peaks appeared due to approximation of a smooth curved surfaces with faceted ones. (For more details on contact formulations and numerical methods, interested readers are referred to the software documentation [7, 8].)

Spatial discretization of the problem has been performed using finite elements of various types. (For details on formulation of various types of finite elements implemented into SIMULIA Abaqus an interested reader is referred to the software documentation [7, 8].)

The concrete core and the steel tube have been discretized through, respectively, 17 280 and 7 680 continuum finite elements of the type C3D8R (see Fig. 2(a)). Each die has been discretized through four rigid finite elements of the type R3D4 with the point mass finite element of the type MASS located at its center. The actuator is discretized through one spring finite element of the type SPRINGA and one dashpot finite element of the type DASHPOTA with the point mass finite element of the type MASS located at its free end. The rebar mats have been discretized through structural finite elements of the type B31 (see Fig. 2(b)). Depending on the particular case, each mat has been meshed with 355, 372, 389, or 480 finite elements.

In all the relevant cases, the welded joints between the rebar rods and the tube have been simulated using a Tie Constraint tool (see Fig. 3(b)). To tie nodes of the beam finite elements with six degrees of freedom to nodes of the continuum finite elements with three degrees of freedom, the internal surface of the tube has been covered with 1 920 surface finite elements of the type SFM3D4R which have zero stiffness. These surface elements have been specified an artificial areal density of 1 kg/m^2 and tied in each node to corresponding nodes on the tube internal surface (see Fig. 3(a)).

Interaction between the reinforcement and the concrete has been simulated through an Embedded Element tool. Translational degrees of freedom of embedded nodes belonging to the reinforcement elements have been constrained to the interpolated values of the corresponding degrees of freedom of the host concrete elements, while rotational degrees of freedom of the embedded nodes have been remained free of constraints. (For more information on the Embedded Element tool an interested reader is referred to the software documentation [7, 8].)

The steel elements of the column have been modeled as made of homogeneous isotropic elastic-plastic non-damageable material with the Maxwell-von Mises yield criterion, an associated

flow rule, and isotropic hardening, that instantly fractures when an accumulated plastic strain reaches its limit value.

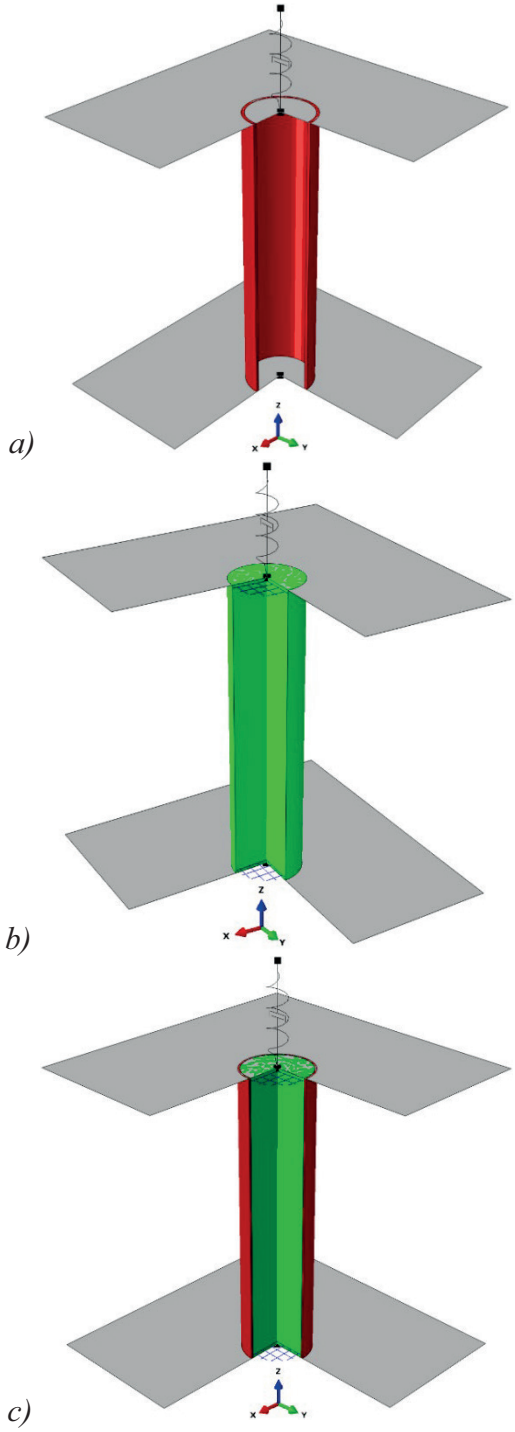

Figure 1. Numerical models for the cases: a) 1-0-30-0; b) 2-B30-0-700, 2-B60-0-700, 2-B90-0-700; c) 1-B30-20-680, 1-B60-20-680, 1-B90-20-680, 2-B30-20-680, 2-B60-20-680, 2-B90-20-680

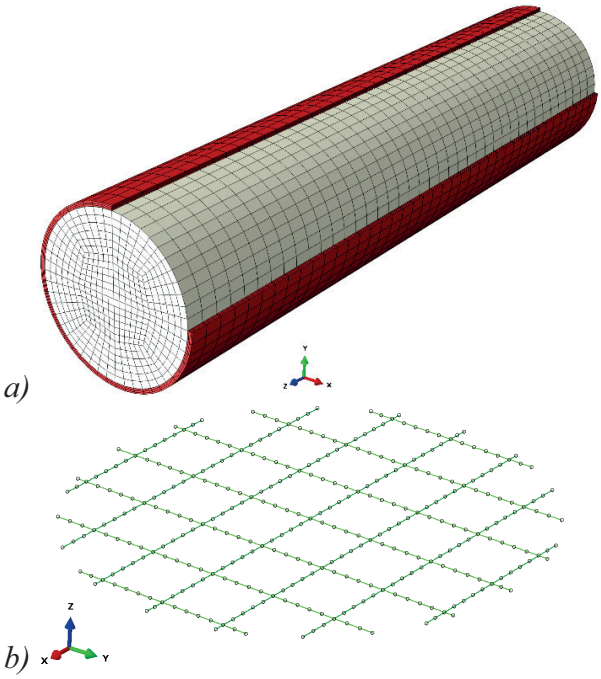

Figure 2. Finite element mesh of: a) the steel tube with the wall thickness of 20 mm and the concrete core (the tube wall is discretized with four continuum finite elements through the thickness); b) the reinforcement mat (nodes are labeled with small black circles)

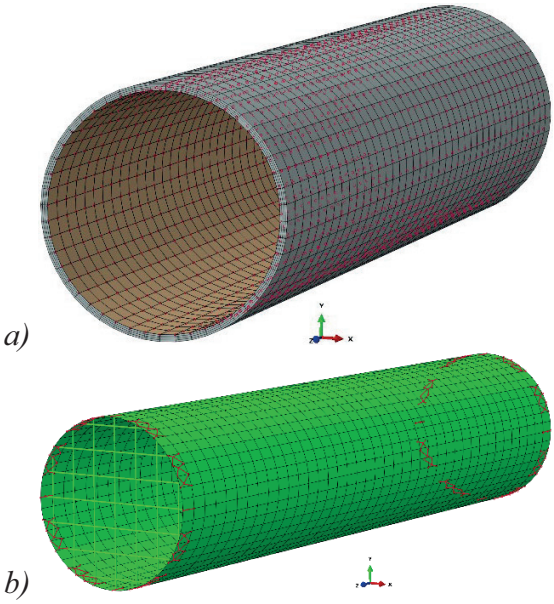

Figure 3. Tie constraints between: a) the auxiliary surface with zero stiffness and the internal tube surface; b) the reinforcement mats and the auxiliary surface (an assembly used in the cases 1-B30-20-680, 1-B60-20-680, and 1-B90-20-680 is presented)

Elastic properties of steel have been described through the Hooke's law for isotropic materials [9]:

$$\hat{\boldsymbol{\sigma}} = \hat{\hat{\mathbf{C}}} : \hat{\boldsymbol{\varepsilon}}_{el} = \lambda \operatorname{tr}\left(\hat{\boldsymbol{\varepsilon}}_{el}\right)\hat{\mathbf{I}} + 2\mu\hat{\boldsymbol{\varepsilon}}_{el}, \tag{2}$$

where $\hat{\boldsymbol{\sigma}}$ is the Cauchy stress tensor, $\hat{\boldsymbol{\varepsilon}}_{el}$ is the Green-Lagrangian elastic strain tensor, $\hat{\hat{\mathbf{C}}}$ is the elastic stiffness tensor of the fourth order, $\hat{\mathbf{I}}$ is the unit tensor, $\operatorname{tr}(\ )$ is the trace operator, and λ and μ are the Lame constants.

The Maxwell-von Mises yield criterion adopted for steel reads [10, 11]:

$$\Phi\left(\hat{\boldsymbol{\sigma}},\ \hat{\mathbf{h}}_k\right) = q - \sigma_y = 0, \tag{3}$$

where $\hat{\mathbf{h}}_k\left(\hat{\boldsymbol{\sigma}},\ \hat{\mathbf{h}}_i\right)\ \ (i,\ k = 1,\ ...,\ N;\ i \neq k)$ are state variables, q is the von Mises equivalent stress, and $\sigma_y \equiv \sigma_y\left(\overline{\varepsilon}_{pl}\right)$ is the yield stress, which, being the function of the accumulated plastic strain measured, as mentioned above, through the von Mises equivalent plastic strain $\overline{\varepsilon}_{pl}$, provides isotropic hardening.

The associated flow rule reads [12]:

$$\dot{\hat{\boldsymbol{\varepsilon}}}_{pl} = \dot{\Lambda}\frac{\partial\Phi}{\partial\hat{\boldsymbol{\sigma}}}, \tag{4}$$

where a dot above a variable hereinafter denotes its material time derivative, and $\dot{\Lambda} \geq 0$ is a scalar function determined from the compatibility condition [12]:

$$\dot{\Phi}\left(\hat{\boldsymbol{\sigma}},\ \hat{\mathbf{h}}_k\right) = 0 \quad (k = 1,\ ...,\ N), \tag{5}$$

which implies that during yielding at some material point the end of a stress vector must stay on a yield surface.

To describe steel strength properties, a simple constant fracture strain criterion, named after Mariotte, Poncelet, and de Saint-Venant [10, 13], has been adopted:

$$\overline{\varepsilon}_{pl} = \overline{\varepsilon}_{pl,f}. \tag{6}$$

It states that fracture in a material point occurs when the accumulated plastic strain (measured through the von Mises equivalent plastic strain $\overline{\varepsilon}_{pl}$) reaches its limit value $\overline{\varepsilon}_{pl,f}$, the von Mises equivalent plastic strain at fracture.

Damage of material microstructure, that occurs during material plastic straining, and its influence onto material elastic properties have not been taken into account within the constructed numerical models. It has been assumed that, once the condition (6) is reached in a material point, the material instantly fractures. Finite elements, at which integration points the fracture criterion had been met, have been eroded from the numerical model, yet their nodes have been retained, in particular as free-floating masses, if all the adjacent finite elements have been eroded.

Properties of the reinforcement material have been taken from the Russian building code SP 63.13330.2018 [1] and are given in Tables 1 and 2.

Table 1. Physical and mechanical properties of the reinforcement material (A500C grade steel according to the Russian standards)

Parameter	Value
Density ρ, $\mathrm{kg/m^3}$	7850
Young's modulus E, GPa	200
Poisson's ratio ν	0.3
Initial yield (true) stress $\sigma_y(0)$, MPa	300.45
Ultimate accumulated (engineering) strain ε_{s2}	0.024693
Von Mises equivalent plastic strain at fracture $\overline{\varepsilon}_{pl,f}$	0.023155
Ultimate (true) stress $\sigma_y\left(\overline{\varepsilon}_{pl,f}\right)$, MPa	307.50

It should be noted here, that material properties in Russian building codes are provided in terms

of engineering stresses and engineering strains. Within the numerical models all stress and strain variables have been defined in terms of true stresses and true strains. Below in the text, both engineering and true stresses and strains are used, so that comments on whether this an engineering or a true variable are given where necessary.

Table 2. True stress-true strain relationship of the reinforcement material under uniaxial tension or compression

σ, MPa	$\overline{\varepsilon}$	$\overline{\varepsilon}_{pl}$
0	0	0
300.45	0.001498876	0
307.50	0.024693	0.023155

Table 3. Physical and mechanical properties of the tube material (C355 grade steel according to the Russian standards) of various thickness t

Parameter	Value	
	$t = 10$ mm	$t = 20,\ 30$ mm
Density ρ, kg/m^3	7850	
Young's modulus E, GPa	206	
Poisson's ratio ν	0.3	
Initial yield (true) stress $\sigma_y(0)$, MPa	280.38	272.36
Ultimate accumulated (engineering) strain ε_f	0.231073	0.225161
Von Mises equivalent plastic strain at fracture $\overline{\varepsilon}_{pl,f}$	0.228308	0.222485
Ultimate (true) stress $\sigma_y\left(\overline{\varepsilon}_{pl,f}\right)$, MPa	569.55	551.21

Properties of the tube material have been taken from the Russian building code SP 16.13330.2017 "Steel structures" [14] and are given in Tables 3-5.

Concrete has been modeled as a homogeneous isotropic elastic-plastic damageable material with the non-associated flow rule, and isotropic hardening and softening using the Concrete Damaged Plasticity (CDP) model based onto the works by Lubliner et al. [2] and Lee and Fenves [15], and implemented into SIMULIA Abaqus software with a thorough description given in the software documentation [7, 8]. Some basic relationships of the CDP model are presented below.

Table 4. True stress-true strain relationship of the tube material of thickness $t = 10$ mm under uniaxial tension or compression

σ, МПа	$\overline{\varepsilon}$	$\overline{\varepsilon}_{pl}$
0	0	0
280.38	0.001358	0
351.01	0.002884	0.001180
359.51	0.026822	0.025076
569.55	0.139783	0.137018
569.55	0.231073	0.228308

Table 5. True stress-true strain relationship of the tube material of thickness t = 20, 30 mm under uniaxial tension or compression

σ, МПа	$\overline{\varepsilon}$	$\overline{\varepsilon}_{pl}$
0	0	0
272.36	0.001320	0
340.95	0.002802	0.001147
348.98	0.026065	0.024371
551.21	0.136049	0.133373
551.21	0.225161	0.222485

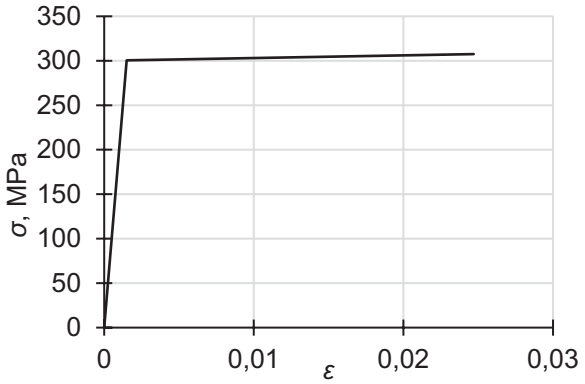

Figure 4. True stress-true strain curve of the reinforcement material (A500C grade steel according to the Russian standards) under uniaxial tension or compression

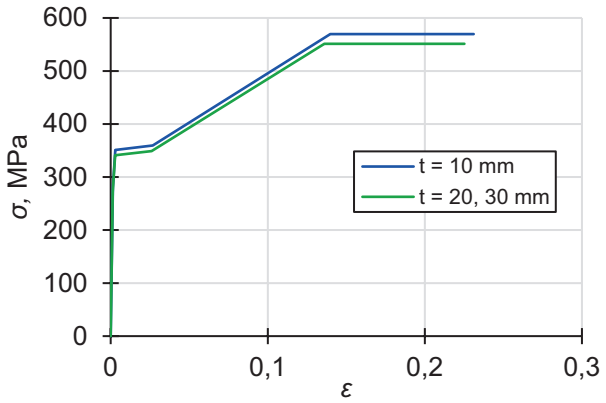

Figure 5. True stress-true strain curve of the tube material (C355 grade steel according to the Russian standards) of various thickness under uniaxial tension or compression

Damage of the material is characterized through two independent variables, d_t and d_c, scalar damage measures under tension and compression, respectively, which are functions of plastic strains, temperature and other field variables. Being increasing functions of the equivalent plastic strains $\overline{\varepsilon}_{pl,t}$ and $\overline{\varepsilon}_{pl,c}$ (accumulated during tension and compression, respectively), these scalar damage measures equal to zero for an intact material and equal to unity for a completely damaged material. Yet, to avoid problems with solution convergence, it is recommended to limit values of the damage variables to 0.99.

Within the CDP model, it is assumed that, under a general stress state, concrete elastic stiffness degradation due to its damage is isotropic. This assumption allows one to use a single scalar measure, d, to describe material damage. Using effective stresses, instead of ordinary stresses, to describe the material stress state, it appears to be possible to keep the general form of the Hooke's law (see Eq. (2)) to describe concrete elastic behaviour:

$$\hat{\bar{\boldsymbol{\sigma}}} = \hat{\mathbf{C}} : \hat{\boldsymbol{\varepsilon}}_{el}, \tag{7}$$

where $\hat{\bar{\boldsymbol{\sigma}}} = \hat{\boldsymbol{\sigma}} / (1-d)$ is the Cauchy effective stress tensor, and a colon denotes a double tensor contraction. The scalar damage measure d is defined in the following way:

$$(1-d) = (1-s_t d_c)(1-s_c d_t), \tag{8}$$

where

$$s_t = 1 - w_t r \quad (0 \le w_t \le 1), \tag{9}$$

$$s_c = 1 - w_c (1-r) \quad (0 \le w_c \le 1), \tag{10}$$

$$r(\hat{\bar{\boldsymbol{\sigma}}}) = \frac{\sum_{i=1}^{3} \langle \bar{\sigma}_i \rangle}{\sum_{i=1}^{3} |\bar{\sigma}_i|} \quad (0 \le r \le 1). \tag{11}$$

Here $\bar{\sigma}_i$ $(i = 1, 2, 3)$ are eigenvalues of the Cauchy effective stress tensor $\hat{\bar{\boldsymbol{\sigma}}}$, $\langle\ \rangle$ is the Macaulay brackets, and w_t and w_c are weight factors, which are considered to be material properties and determine the extent of stiffness recovery of the damaged material during stress sign change from compression to tension and from tension to compression, respectively. For instance, the value $w_c = 1$ means that material damage accumulated during tension cycles has no influence onto its compressive stiffness. And vice versa, the $w_c = 0$ means that material damage accumulated during tension cycles has a

direct effect onto its compressive stiffness. Intermediate values of the factor w_c correspond to partial compressive stiffness recovery. The above becomes valid for the factor w_t through simple replacement of the term "tension" by "compression", and vice versa. (For more details, an interested reader is referred to the software documentation [7, 8].)

It is commonly assumed that, when the stress sign changes from tension to compression, complete concrete stiffness recovery occurs through the crack closing mechanism, that is $w_c = 1$. At the same time, it is assumed that in the opposite case, when the stress sign changes from compression to tension, there is no stiffness recovery, i.e. $w_t = 0$.

It must be emphasized that, within the CDP model, stress state parameters are defined in terms of the effective stresses and correspondingly denoted with an over-bar. (This notation is applied only for stress variables. So, one should not confuse it with the over-bar used to denote the equivalent strain.)

Despite all the calculations within the material code are performed using the equivalent plastic strains $\overline{\varepsilon}_{pl,t}$ and $\overline{\varepsilon}_{pl,c}$ (accumulated during tension and compression, respectively), that refer to the damaged state of a material, to input material damage properties, the equivalent cracking strain $\overline{\varepsilon}_{ck,t}$ and the equivalent inelastic strain $\overline{\varepsilon}_{in,c}$, that refer to the intact state of a material, are utilized for tension and compression, respectively. The relationships between these strain measures under uniaxial loading conditions are the following:

$$\overline{\varepsilon}_{pl,t} = \overline{\varepsilon}_{ck,t} - \frac{d_t}{\left(1-d_t\right)}\frac{\sigma_t}{E_0}, \tag{12}$$

$$\overline{\varepsilon}_{pl,c} = \overline{\varepsilon}_{in,c} - \frac{d_c}{\left(1-d_c\right)}\frac{\sigma_c}{E_0}, \tag{13}$$

where E_0 is the Young's modulus of an intact material, and σ_t and σ_c are the absolute values of tensile and compressive stress, respectively. (For some graphical representation of the given relationships, an interested reader is referred to the software documentation [7, 8].)

In the CDP model, the yield criterion developed by Lubliner et al. [2] and modified by Lee and Fenves [15], to take into account that concrete properties under tension and compression are different, is implemented:

$$\Phi\left(\hat{\bar{\boldsymbol{\sigma}}},\ \hat{\mathbf{h}}_k\right) = \frac{1}{1-\alpha}\left(\sqrt{3\overline{J}_2} + \alpha\overline{I}_1 + \beta\left\langle\overline{\sigma}_1\right\rangle - \gamma\left\langle-\overline{\sigma}_1\right\rangle\right) - \overline{\sigma}_c = 0 \quad \left(k = 1,\ \ldots,\ n\right), \tag{14}$$

where

$$\beta = \frac{\overline{\sigma}_c}{\overline{\sigma}_t}\left(1-\alpha\right) - \left(1+\alpha\right), \tag{15}$$

$\overline{I}_1$ is the first invariant of the Cauchy effective stress tensor $\hat{\bar{\boldsymbol{\sigma}}}$, $\overline{J}_2$ is the second invariant of the effective stress deviator $\hat{\bar{\mathbf{S}}}$, α and γ are non-dimensional material parameters, and $\overline{\sigma}_t \equiv \overline{\sigma}_t\left(\overline{\varepsilon}_{pl,t}\right)$ and $\overline{\sigma}_c \equiv \overline{\sigma}_c\left(\overline{\varepsilon}_{pl,c}\right)$ are the effective elastic limits under uniaxial tension and compression, respectively.

The parameter α can be determined through the following relationship:

$$\alpha = \frac{\sigma_{b0} - \sigma_{c0}}{2\sigma_{b0} - \sigma_{c0}}, \tag{16}$$

where σ_{c0} is the initial elastic limit of a material under uniaxial compression, σ_{b0} is the initial elastic limit of a material under uniform biaxial compression. As experiments revealed [2], the ratio $\sigma_{b0}/\sigma_{c0} \in \left[1.10,\ 1.16\right]$ is common for concrete, that yields $\alpha \in \left[0.08,\ 0.12\right]$.

The parameter γ can be defined as follows:

$$\gamma = \frac{3\left(1-K_c\right)}{2K_c-1}, \tag{17}$$

where for points on the yield surface (14), provided $\bar{\sigma}_1 < 0$ and $\bar{I}_1$ takes some compatible value,

$$K_c = \frac{\sqrt{3\bar{J}_2}\Big|_{\bar{\theta}=0}}{\sqrt{3\bar{J}_2}\Big|_{\bar{\theta}=\pi/3}}. \tag{18}$$

Here $\bar{\theta}$ is the effective Lode angle. A typical value [2] for concrete is $K_c = 2/3$, that yields $\gamma = 3$.

In the CDP model the non-associated flow rule is adopted:

$$\dot{\hat{\boldsymbol{\varepsilon}}}_{pl} = \dot{\Lambda}\frac{\partial \Pi}{\partial \hat{\bar{\boldsymbol{\sigma}}}}, \tag{19}$$

where the plastic potential Π is defined through the hyperbolic function:

$$\Pi\left(\hat{\bar{\boldsymbol{\sigma}}},\ \hat{\mathbf{h}}_k\right) = \sqrt{\left(\zeta\sigma_{t0}\tan\left(\psi\right)\right)^2 + 3\bar{J}_2} + \frac{1}{3}\bar{I}_1\tan\left(\psi\right) \qquad \left(k = 1,\ \ldots,\ n\right). \tag{20}$$

Here ψ is the dilation angle at high confining pressure, ζ is a parameter, referred to as the eccentricity, that defines the rate at which the function (20) approaches the asymptote.

(For some graphical information on the yield surface (14) and the plastic flow potential surface (20), interested readers are referred to the software documentation [7, 8].)

To facilitate solution convergence, a viscoplastic regularization of the constitutive equations, viz. a generalization of the Duvaut-Lions regularization [16], is implemented into the CDP model. Instead of an elastic-plastic material, an elastic-viscoplastic one is considered, so that the compatibility condition (5) may not be strictly met, i.e. stresses are permitted to be outside the yield surface (14). Governing equations are as follows:

$$\dot{\hat{\boldsymbol{\varepsilon}}}_{vpl} = \frac{1}{\mu}\left(\hat{\boldsymbol{\varepsilon}}_{pl} - \hat{\boldsymbol{\varepsilon}}_{vpl}\right), \tag{21}$$

$$\dot{d}_v = \frac{1}{\mu}\left(d - d_v\right). \tag{22}$$

Here $\hat{\boldsymbol{\varepsilon}}_{vpl}$ is the viscoplastic strain tensor, $\hat{\boldsymbol{\varepsilon}}_{pl}$ is the plastic strain tensor evaluated for the original elastic-plastic material, d_v is the viscous scalar damage measure, d is the scalar damage measure evaluated for the original elastic-plastic material, and μ is the viscosity parameter, that represents the relaxation time of an elastic-viscoplastic material. For such an artificial elastic-viscoplastic material, the generalized Hooke's law (7) takes the following form:

$$\hat{\boldsymbol{\sigma}} = \left(1-d_v\right)\hat{\hat{\mathbf{C}}} : \left(\hat{\boldsymbol{\varepsilon}} - \hat{\boldsymbol{\varepsilon}}_{vpl}\right). \tag{23}$$

It must be emphasized, that in the CDP model the total damage of a material is not allowed for, and, hence, there is no element erosion during solution of any problem. While cracks cannot be modeled explicitly with such restrictions, they still can be simulated through material stiffness degradation due to damage along some planes. At the same time, with the stiffness recovery during stress sign change, implemented into the material model, and without element erosion, which forms a crack that have a finite dimension in the direction of the normal to its edges, it is possible to accurately simulate crack opening and closing.

Adopted values of the CDP model parameters for various concrete grades are given in Table 6. Some of them have been taken from Russian building code SP 63.13330.2018 "Concrete and

reinforced concrete structures. General provisions" [1], while for other parameters recommended values have been defined (see the software documentation [7, 8]).

Table 6. Physical and mechanical properties of concrete of various grades

Parameter	Value		
	B30	B60	B90
Density ρ, kg/m^3	2500		
Poisson's ratio ν	0.2		
Young's modulus E, GPa	32.5	39.5	42.5
Dilation angle ψ, °	30		
Eccentricity ζ of the plastic flow potential Π	0.1		
Ratio σ_{b0}/σ_{c0} of initial elastic limit under uniform biaxial compression to initial elastic limit under uniaxial compression	1.16		
K_c	0.67		
Relaxation time μ, s	0		
Extent w_c of stiffness recovery of the damaged material during stress sign change from tension to compression	1.0		
Extent w_t of stiffness recovery of the damaged material during stress sign change from compression to tension	0		

Adopted stress-strain and damage-strain relationships for various concrete grades are presented in Tables 7-12 and Figs. 6-11. The stress-strain relationships are based onto data from Russian building code SP 63.13330.2018 "Concrete and reinforced concrete structures. General provisions" [1], which have been recalculated in terms of true stresses and true strains. The damage-strain relationships, also specified in terms of true strains, have been established based on the author's experience and provide scalar damage measures d_t and d_c being increasing functions of the equivalent plastic strains $\overline{\varepsilon}_{pl,t}$ and $\overline{\varepsilon}_{pl,c}$, respectively.

Table 7. True stress-true strain and damage-true strain relationships for B30 grade concrete under uniaxial compression

σ_c, MPa	ε_c	$\varepsilon_{in,c}$	d_c
0	0	0	0
10.203	0.0003138	0	0
17.034	0.0019980	0.0014739	0.25
17.060	0.0034939	0.0029690	0.55
0.3417	0.0049875	0.0049770	0.99

Table 8. True stress-true strain and damage-true strain relationships for B30 grade concrete under uniaxial tension

σ_t, MPa	ε_t	$\varepsilon_{ck,t}$	d_t
0	0	0	0
0.6900	0.00002123	0	0
1.1501	0.00010000	0.00006461	0.25
1.1502	0.00014999	0.00011460	0.55
0.0230	0.00149888	0.00149817	0.99

Table 9. True stress-true strain and damage-true strain relationships for B60 grade concrete under uniaxial compression

σ_c, MPa	ε_c	$\varepsilon_{in,c}$	d_c
0	0	0	0
19.810	0.0005011	0	0
33.066	0.0019980	0.0011609	0.25
33.116	0.0034939	0.0026555	0.55
0.6633	0.0049875	0.0049707	0.99

Table 10. True stress-true strain and damage-true strain relationships for B60 grade concrete under uniaxial tension

σ_t, MPa	ε_t	$\varepsilon_{ck,t}$	d_t
0	0	0	0
1.0800	0.00002734	0	0
1.8002	0.00010000	0.00005442	0.25
1.8003	0.00014999	0.00010441	0.55
0.0361	0.00149888	0.00149796	0.99

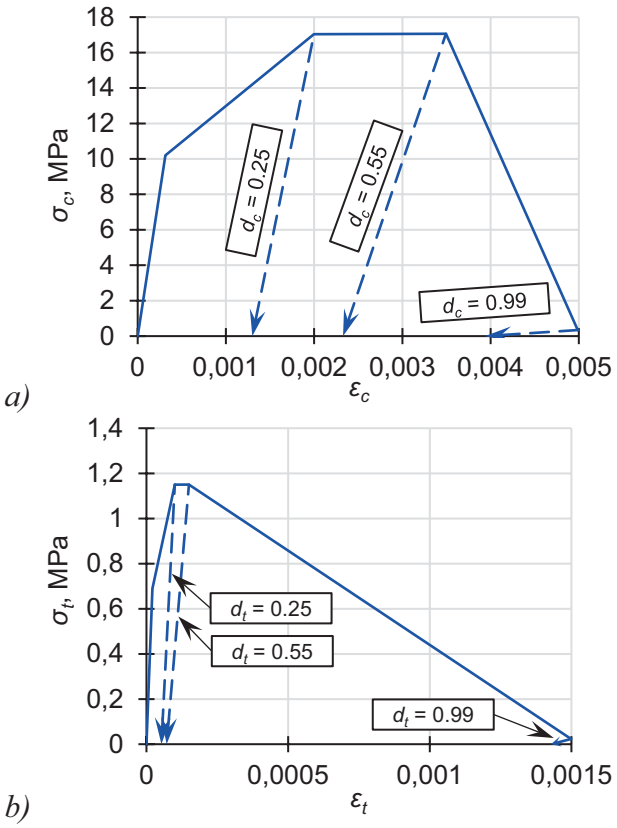

Figure 6. True stress-true strain curves for B30 grade concrete under: a) uniaxial compression; b) uniaxial tension

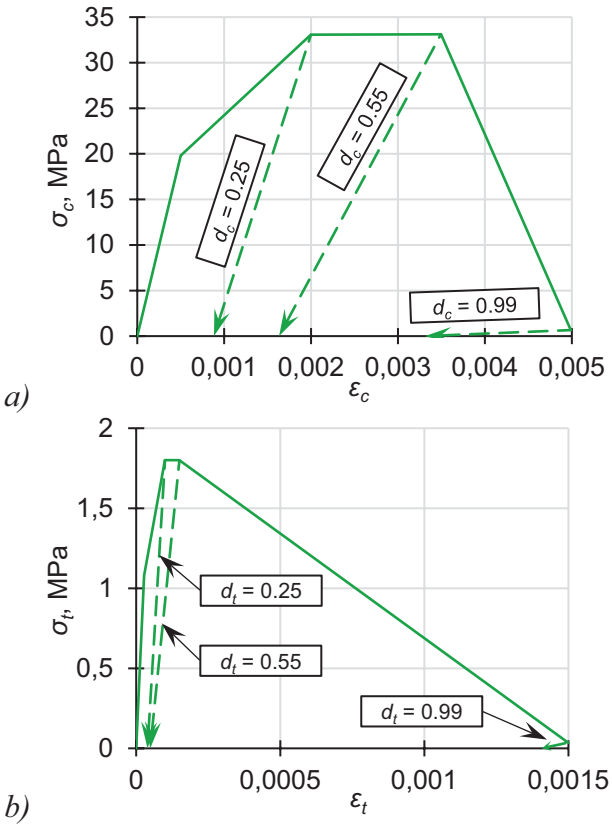

Figure 7. True stress-true strain curves for B60 grade concrete under: a) uniaxial compression; b) uniaxial tension

Table 11. True stress-true strain and damage-true strain relationships for B90 grade concrete under uniaxial compression

σ_c, MPa	ε_c	$\varepsilon_{in,c}$	d_c
0	0	0	0
26.416	0.0006210	0	0
44.088	0.0019980	0.0009606	0.25
44.131	0.0029656	0.0019272	0.55
0.8844	0.0049875	0.0049667	0.99

Table 12. True stress-true strain and damage-true strain relationships for B90 grade concrete under uniaxial tension

σ_t, MPa	ε_t	$\varepsilon_{ck,t}$	d_t
0	0	0	0
1.2900	0.00003035	0	0
2.1502	0.00010000	0.00004940	0.25
2.1503	0.00014999	0.00009939	0.55
0.0431	0.00149888	0.00149786	0.99

4. RESULTS

For each of the 33 cases considered a force-displacement curve and stress-strain states at different levels of axial compressive load, in particular limit states of the first group corresponding to local maxima of the force-displacement curve. Several force-displacement curves are presented in Fig. 12.

It has been revealed that the limit states are qualitatively similar for the cases with similar features. For instance, in the cases when vertical load acts only onto the concrete (irrespective of whether there is the steel tube or not), there is only one extremum on the force-displacement curve (see Fig. 12(c), (d)) and only one limit state of the first group corresponding to it, at which strains throughout the concrete part of some cross-section along the column reach the value of

limit strain of concrete under short-time compression, ε_{b2}.

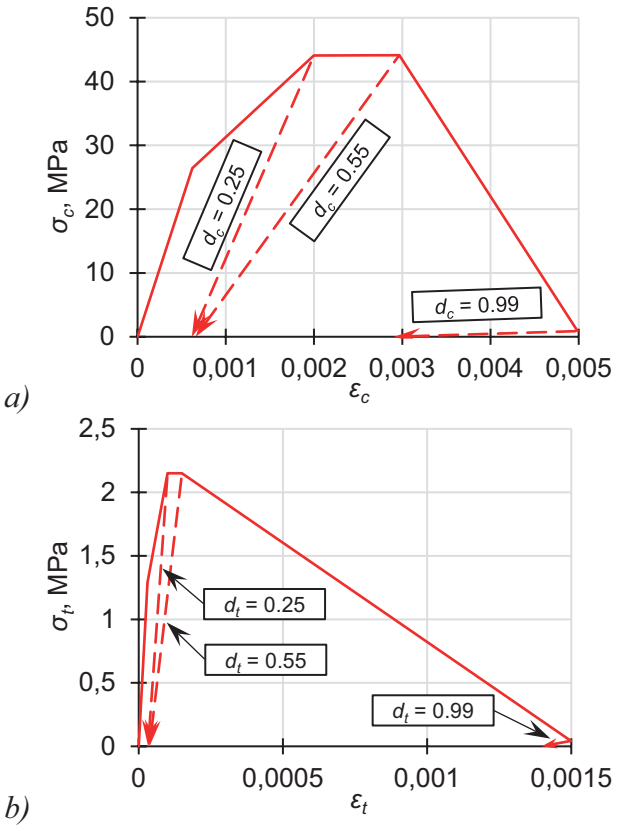

Figure 8. True stress-true strain curves for B90 grade concrete under: a) uniaxial compression; b) uniaxial tension

Such a state is also the first one of the first group of limit states for the cases when vertical load is applied onto both steel tube and concrete core. In all such cases the corresponding force-displacement curves have two extrema (see Fig. 12(b)). The second limit state of the first group corresponds to failure of the steel tube at some circumferential cross-section along the column.

In the cases when there is no concrete core and vertical load acts only onto the steel tube, also two limit states of the first group can be singled out, yet the corresponding force-displacement curves also have only one extremum (see Fig. 12(a)). The first limit state of the first group takes place when some cross-section along the column reaches plastic state throughout its area. The second limit state of the first group, as for the set of cases mentioned above, corresponds to failure of the steel tube at some circumferential cross-section along the column and is identified by the local maximum of the force-displacement curve.

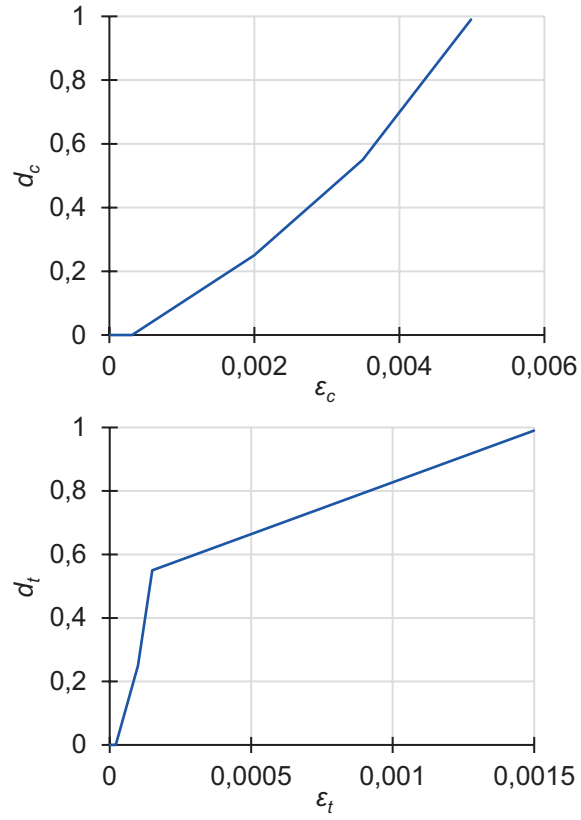

Figure 9. Damage-true strain curves for B30 grade concrete under: a) uniaxial compression; b) uniaxial tension

Examples of the limit states of the first group obtained in the considered cases are given in Fig. 13.

It is worth noting that the problem formulation when the vertical load acts only onto the concrete core can be translated into practice only within limited deformation of concrete in the vertical direction. After some deformation of the concrete core such a column in the vertical direction structural elements below and above it (for instance, floors or girders) inevitably come into contact with the ends of the steel tube. Evidently, this will change the structural scheme of the column and make it similar to the one when the vertical load from the very beginning acts onto the ends of both the steel tube and the concrete core, so that the second limit state of the first

group, viz. failure of the steel tube at some circumferential cross-section along the column, will eventually appear, if the vertical loading continues.

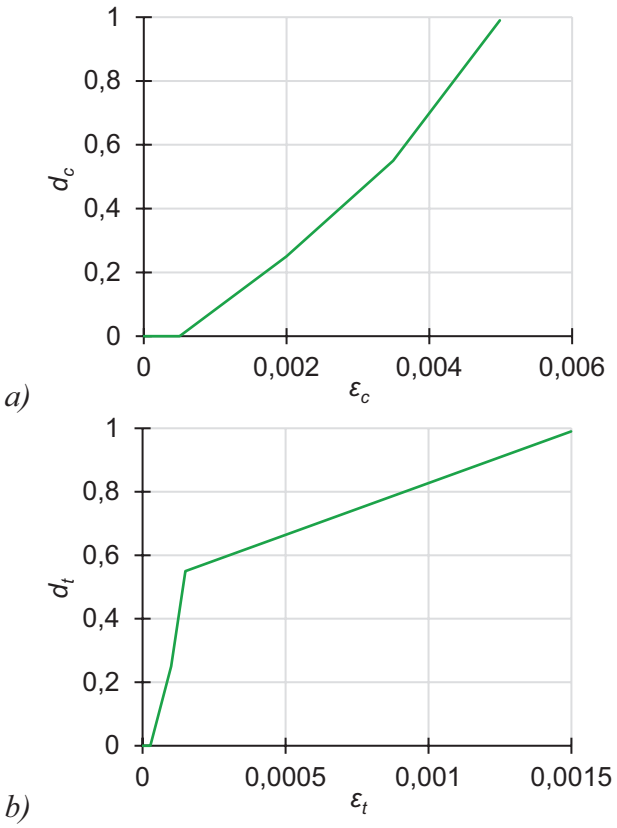

Figure 10. Damage-true strain curves for B60 grade concrete under: a) uniaxial compression; b) uniaxial tension

Moreover, in all the cases with the steel tube and the concrete core failure of the tube at some circumferential cross-section along the column does not immediately lead to a complete loss of structural element capacity. Even the fractured tube continues retaining the concrete core, which is totally crushed by this point, until it will be ruptured by internal pressure created by the concrete crumbles, that can be even considered as the third limit state of the first group.

Since both of the issues mentioned above take place only under very high deformation of the concrete core in the vertical direction, they have not been considered within the present research, because it has no practical sense.

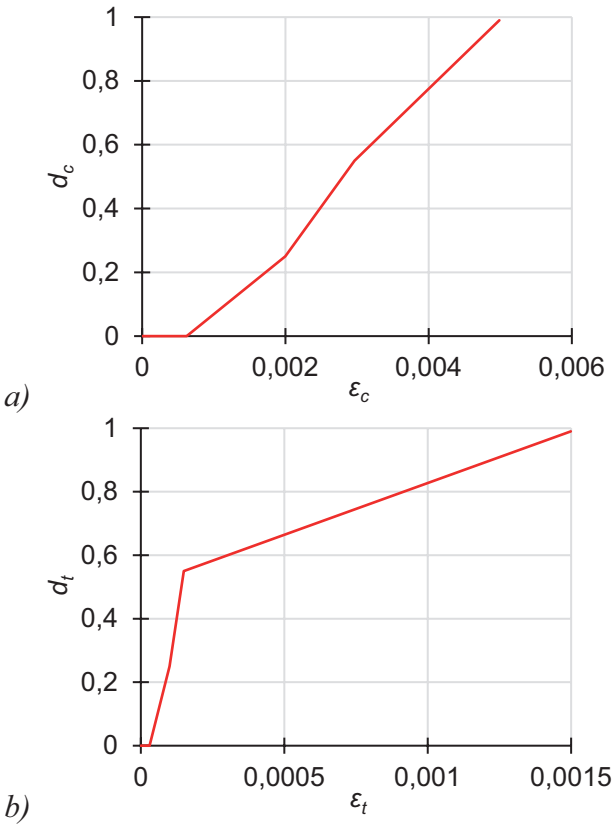

Figure 11. Damage-true strain curves for B90 grade concrete under: a) uniaxial compression; b) uniaxial tension

Parameters of the limit states of the first group calculated for all the 33 cases considered are given in Tables 13 and 14.

Below, in Figs. 14, 16, and 18, force-displacement curves are presented for the simulated cases, grouped by different shared features to facilitate their comparison and estimation of influence of various problem parameters onto the steel tube confined concrete column strength.

In Figs. 15, 17, and 19, parameters of the limit states of the first group for the cases given in Figs. 14, 16, and 18, respectively, are depicted. Again, grouping the cases by different shared features allows one to identify, which problem parameters have the largest effect onto the steel tube confined concrete column strength and whether their influence is monotonic or not.

Table 13. Parameters of the first limit state of the first group calculated for all the 33 cases

Case No.	Displacement of the top die, m	Load, kN
1-0-10-0	0.0113	7851.377
1-B30-10-700	0.0079	16867.18
1-B60-10-700	0.0083	21739.31
1-B90-10-700	0.0051	22855.93
1-0-20-0	0.0106	15001.11
1-B30-20-680	0.0081	24701.27
1-B60-20-680	0.0079	28890.05
1-B90-20-680	0.0056	29228.33
1-0-30-0	0.0106	22199.15
1-B30-30-660	0.0106	32186.44
1-B60-30-660	0.0083	35736.06
1-B90-30-660	0.0057	35078.73
2-B30-0-720	0.0032	5187.777
2-B60-0-720	0.0031	9260.619
2-B90-0-720	0.0027	11707.21
2-B30-0-700	0.0035	4856.732
2-B60-0-700	0.0033	8747.732
2-B90-0-700	0.0032	11234.92
2-B30-0-680	0.0040	4761.817
2-B60-0-680	0.0033	8275.723
2-B90-0-680	0.0028	10379.59
2-B30-0-660	0.0034	4195.609
2-B60-0-660	0.0034	7837.114
2-B90-0-660	0.0029	9879.836
2-B30-10-700	0.0108	19250.89
2-B60-10-700	0.0104	24840.17
2-B90-10-700	0.0082	24992.45
2-B30-20-680	0.0125	29500.08
2-B60-20-680	0.0127	34545.12
2-B90-20-680	0.0101	31897.50
2-B30-30-660	0.0155	39266.76
2-B60-30-660	0.0150	43777.00
2-B90-30-660	0.0107	36855.08

In Fig. 20, and Tables 15 and 16 a steel tube confined concrete column strength increase factor k is given. It has been calculated through the following relation:

$$k = F/F_0 , \qquad (24)$$

where F is the steel tube confined concrete column strength, and F_0 is the strength of the column made of plain concrete with the diameter equal to that of the concrete core of the steel tube confined concrete column.

Table 14. Parameters of the second limit state of the first group calculated for the relevant cases

Case No.	Displacement of the top die, m	Load, kN
1-0-10-0	0.5648	15972.75
1-B30-10-700	0.5573	24272.70
1-B60-10-700	0.5560	25232.82
1-B90-10-700	0.5462	25434.39
1-0-20-0	0.4084	27563.00
1-B30-20-680	0.5046	37025.38
1-B60-20-680	0.5056	38384.91
1-B90-20-680	0.5130	39368.96
1-0-30-0	0.3573	37933.93
1-B30-30-660	0.3857	45513.13
1-B60-30-660	0.3878	47007.78
1-B90-30-660	0.3836	47231.08

Table 15. Steel tube confined concrete column strength increase relative to that of the column made of plain concrete in the cases, when the vertical load acts onto both the steel tube and the concrete core

Tube thickness, mm	Concrete grade		
	B30	B60	B90
0	1	1	1
10	3.47	2.49	2.03
20	5.19	3.49	2.82
30	7.67	4.56	3.55

Table 16. Steel tube confined concrete column strength increase relative to that of the column made of plain concrete in the cases, when the vertical load acts only onto the concrete core

Tube thickness, mm	Concrete grade		
	B30	B60	B90
0	1	1	1
10	3.96	2.84	2.22
20	6.20	4.17	3.07
30	9.36	5.59	3.73

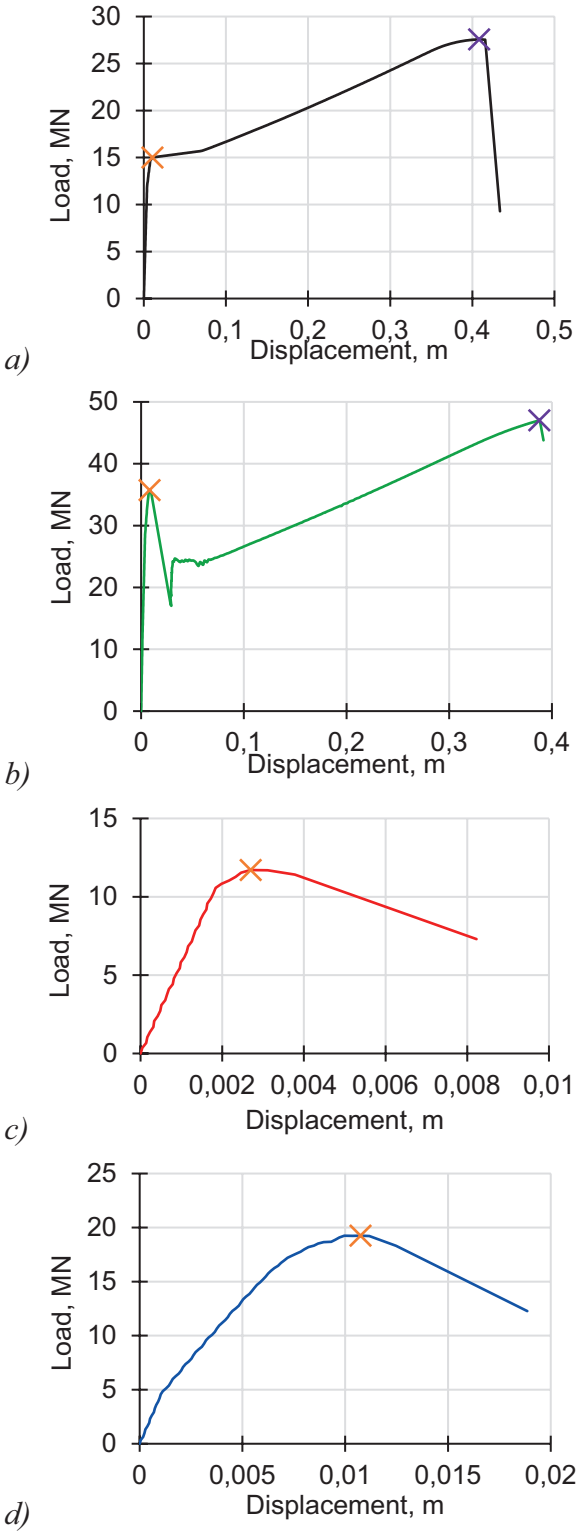

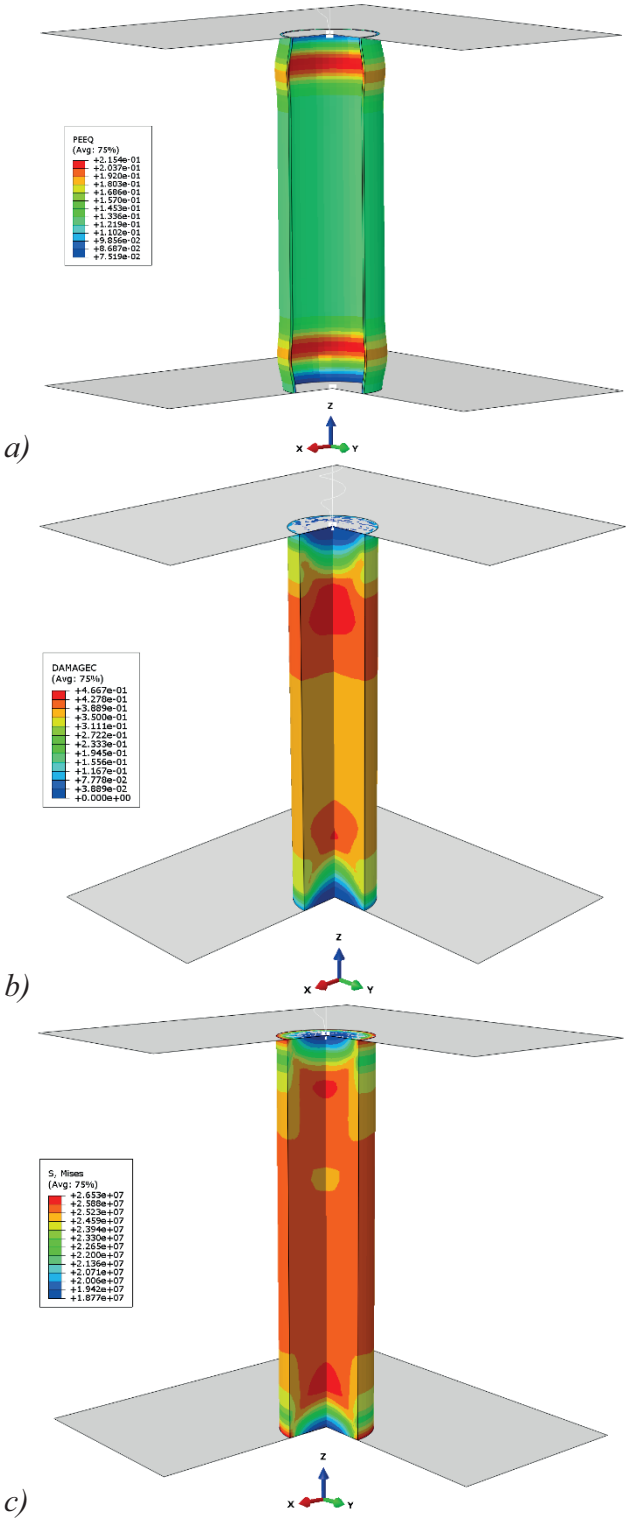

Figure 12. Force-displacement curves obtained for the cases: a) 1-0-20-0; b) 1-B60-30-660; c) 2-B90-0-720; d) 2-B30-10-700 (limit states of the first group are marked with orange and purple oblique crosses)

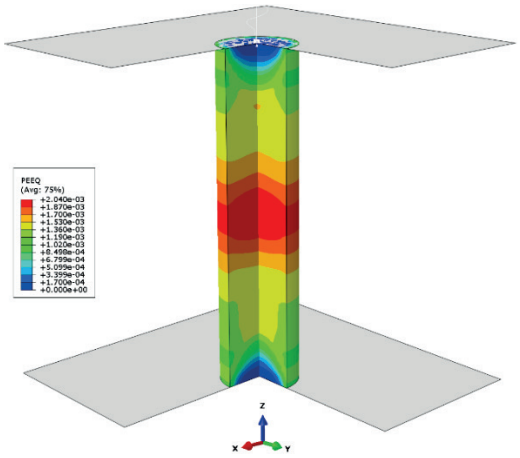

d)

Figure 13. Limit states of the first group obtained in different cases: a) the von Mises equivalent plastic strain $\overline{\varepsilon}_{pl}$ prior to tube failure in the case 1-0-20-0; b) scalar measure of concrete damage due to compression d_c prior to concrete core failure in the case 1-B60-30-660; c) the von Mises equivalent stress q prior to concrete failure in the case 2-B90-0-720; d) the von Mises equivalent plastic strain $\overline{\varepsilon}_{pl}$ in the concrete core prior to its failure in the case 2-B30-10-700

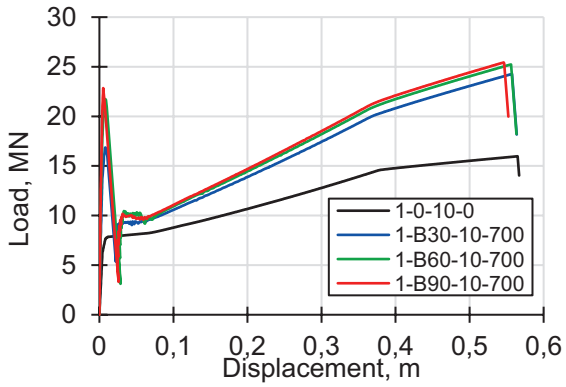

a)

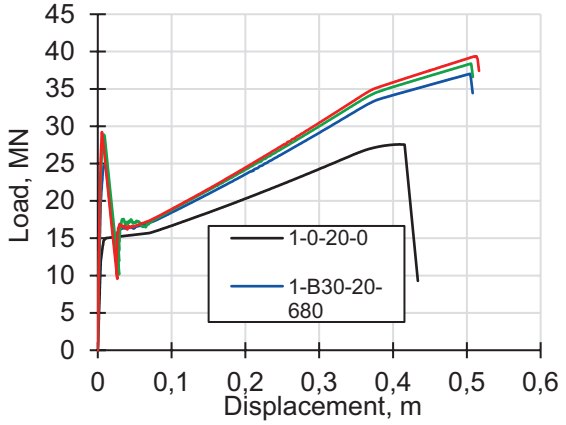

b)

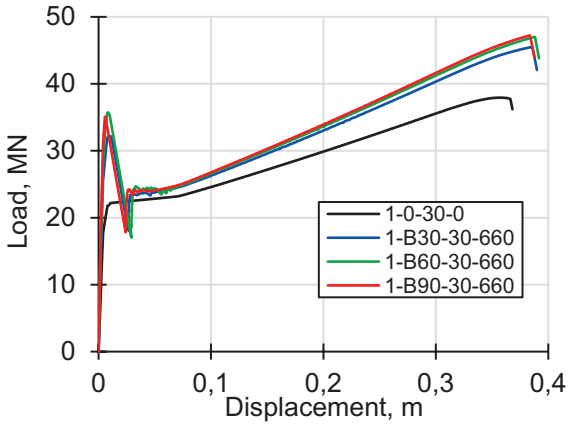

c)

Figure 14. Force-displacement curves for different groups of cases: a) 10 mm thick steel tube; b) 20 mm thick steel tube; c) 30 mm thick steel tube

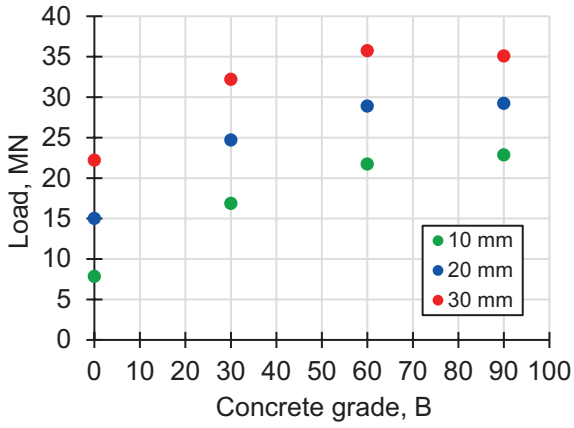

a)

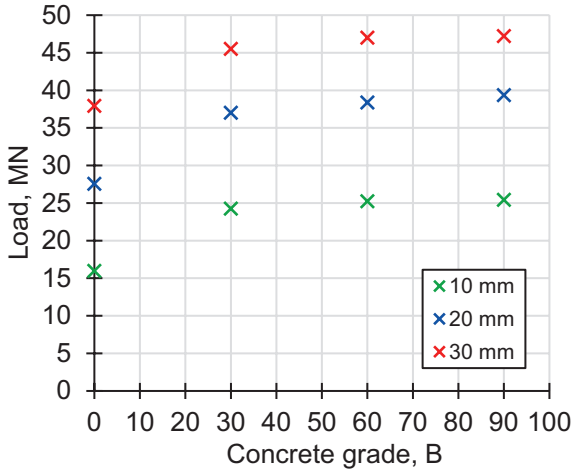

b)

Figure 15. Influence of the concrete grade and the tube thickness onto parameters of the limit states of the first group in the cases, which force-displacement curves are given in Fig. 14: a) the first limit state of the first group; b) the second limit state of the first group

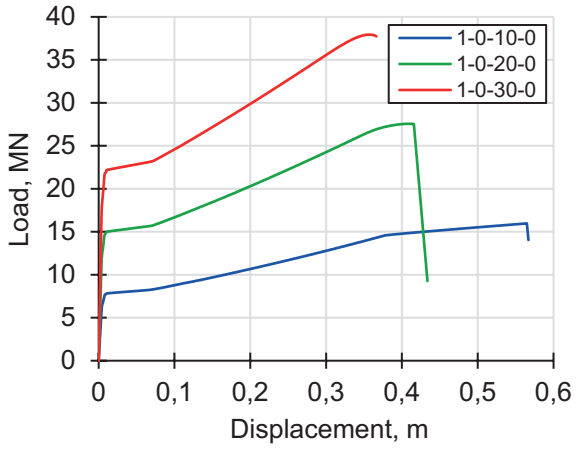

a)

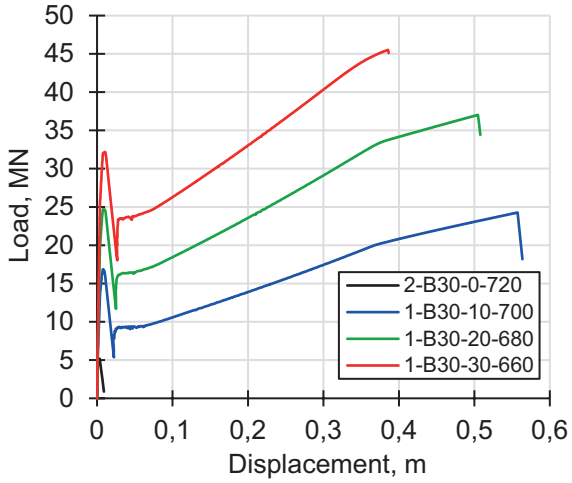

b)

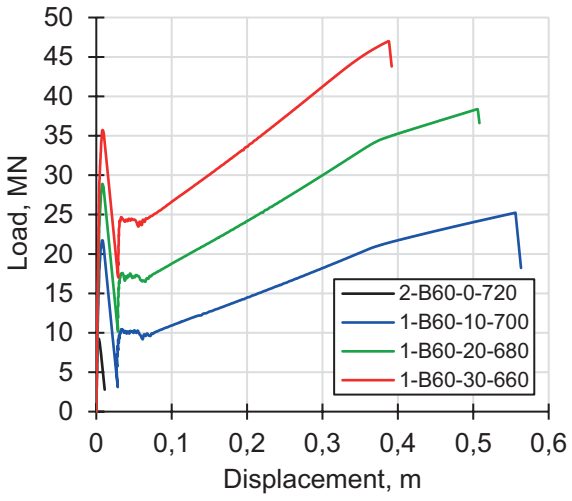

c)

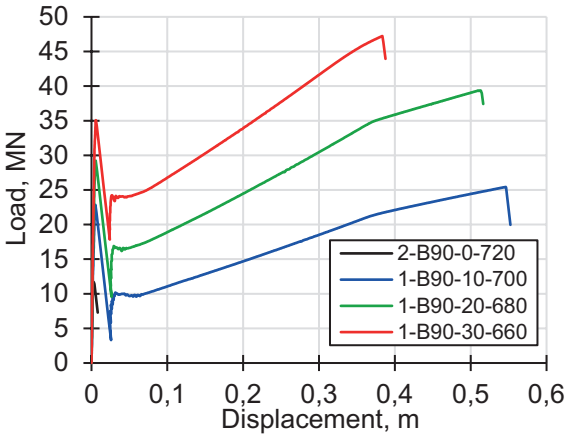

d)

Figure 16. Force-displacement curves for different groups of cases: a) no concrete; b) B30 grade concrete; c) B60 grade concrete; d) B90 grade concrete

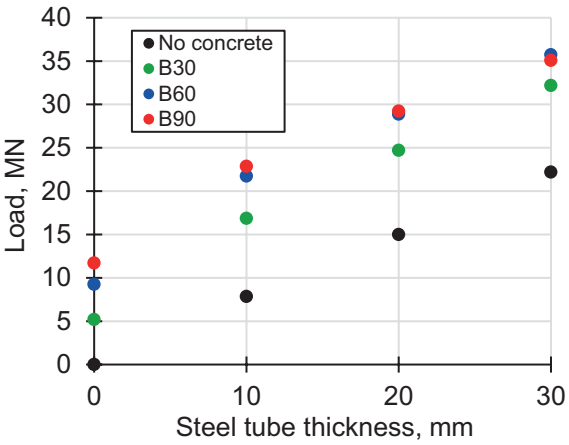

a)

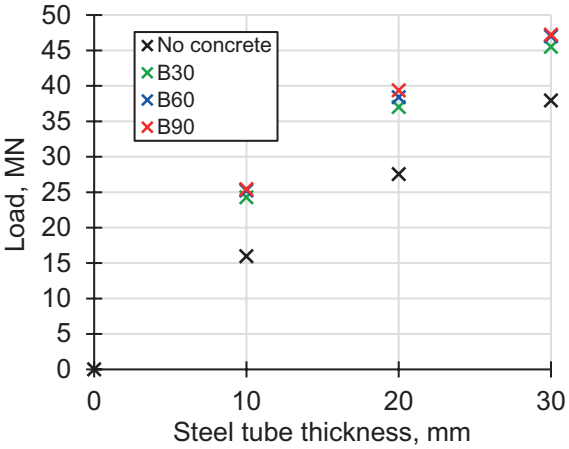

b)

Figure 17. Influence of the concrete grade and the tube thickness onto parameters of the limit states of the first group in the cases, which force-displacement curves are given in Fig. 16: a) the first limit state of the first group; b) the second limit state of the first group

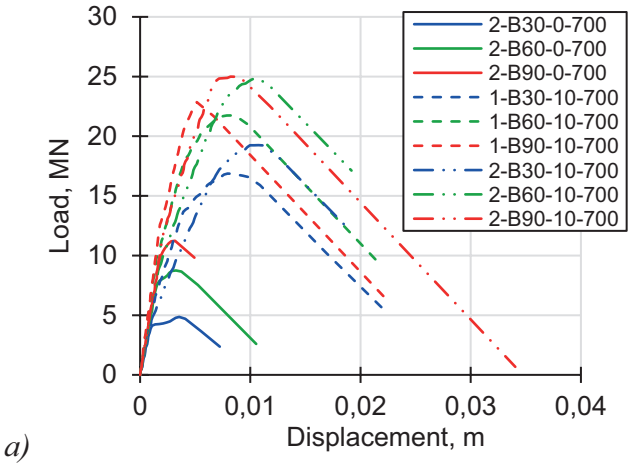

a)

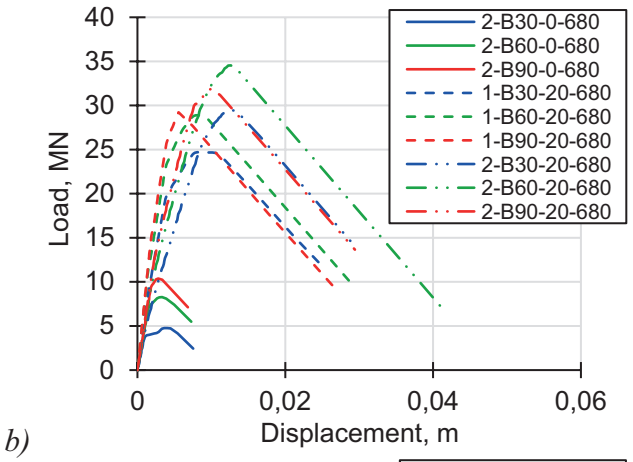

b)

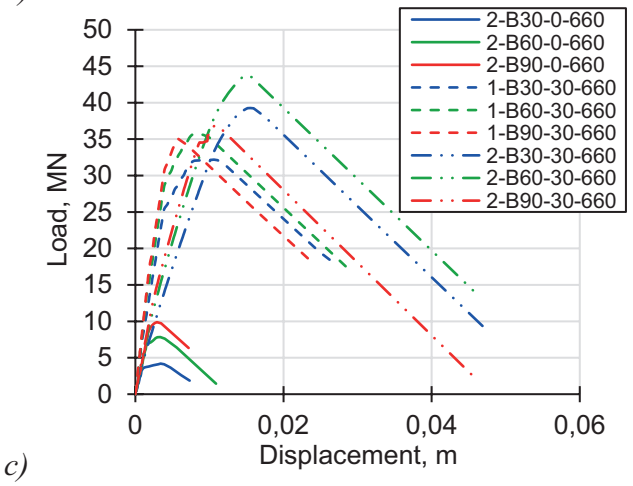

c)

Figure 18. Force-displacement curves for different groups of cases: a) concrete core diameter of 700 mm; b) concrete core diameter of 680 mm; c) concrete core diameter of 660 mm

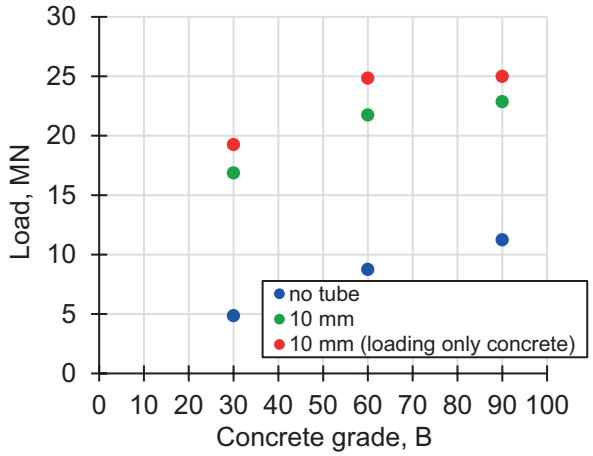

a)

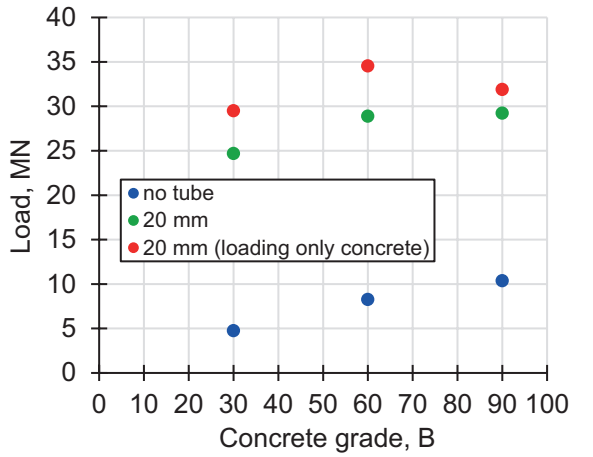

b)

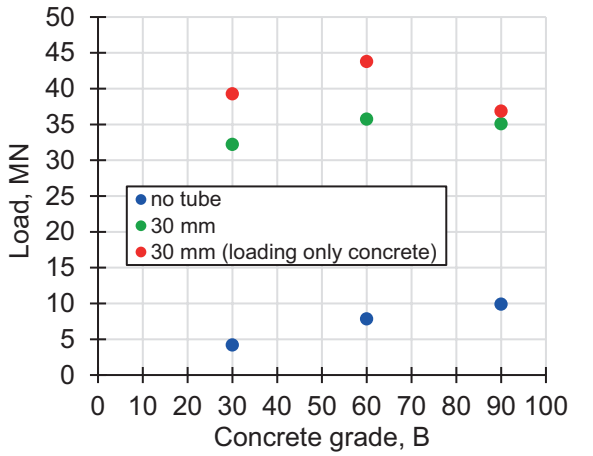

c)

Figure 19. Parameters of the first limit state of the first group in the cases, which force-displacement curves are given in: a) Fig. 10(a); b) Fig. 10(b); c) Fig. 10(c)

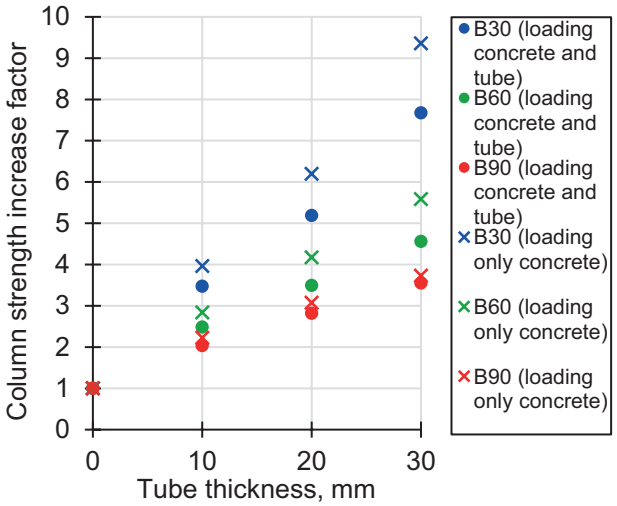

Figure 20. Steel tube confined concrete column strength increase relative to that of the column made of plain concrete

5. DISCUSSION

First of all, the very concept of the steel tube confined concrete column has been confirmed to be viable and effective. Taking the calculated values of the ultimate load for the first limit state of the first group (see Table 13) in the cases, for instance, 1-0-20-0 and 2-B30-0-680, that are 15 001.11 kN and 4 761.82 kN, respectively, one can see that their sum, which equals to 19 762.93 kN, is less than the values of the ultimate load (for the first limit state of the first group) in the relevant cases 1-B30-20-680 and 2-B30-20-680, that are 24701.27 kN and 29500.08 kN, respectively. The synergy effect of the steel tube and the concrete core is clear. (Using Table 13, one can ascertain that this is true for all other combinations.)

Several important conclusions concerning effects of concrete grade and steel tube thickness onto column strength can be made already from Figs. 14 and 15. In the cases, when the vertical load acts onto the ends of both the concrete core and the steel tube, the strength of the steel tube confined concrete column, measured through parameters of both the first and the second limit states of the first group, increases (as anticipated) with the tube thickness and (or) concrete grade. Yet, influence of these problem parameters is non-linear.

Considering the first limit state of the first group and comparing the ultimate vertical load for the steel tube confined concrete column with that for the tubular steel column, one can see, that concrete core contribution to the column strength remains almost the same in absolute terms with the tube thickness increase for all the considered concrete grades, but diminishes in relative terms. Moreover, increasing the concrete grade above B60 has insignificant (even negative in the case 1-B90-30-660) effect onto the column strength (see also Fig. 17(a)). The reason is simple. The guideline value of the limit strain under short-time compression ε_{b2} decreases with the grade for the concrete grades above B60, i.e. the high-strength concrete is more brittle. And this limit strain decrease (almost) balances out the increase of the concrete compressive strength with regard to the amount of inelastic work being able to be done by the concrete of a particular grade.

Looking at the shape of the force-displacement curves given in Fig. 14, it becomes evident that the second limit state of the first group is governed by the strength of the steel tube. Yet, the very existence of the concrete core has a significant positive effect onto the tube strength, and the thinner is the tube, the larger is the effect. Despite the concrete core is totally crushed by the time the second limit state of the first group is reached, it still has a residual bulk stiffness and facilitates tube stability. Since the second limit state of the first group is governed by the tube buckling, such an effect caused by the concrete core is unsurprising. At the same time, the concrete grade has a minor effect onto the parameters of the second limit state of the first group, that is clearly seen in Fig. 17(b). It is also expected. The bulk stiffness of the concrete crumbles is only a small fraction of that of intact concrete, so that the difference between various concrete grades is small in absolute terms.

One can see in Figs. 14 and 16 that, in the cases when the vertical load acts onto both the steel tube and the concrete core, the value of the displacement corresponding to the second limit state of the first group decreases with the tube thickness, and it is almost independent of the

concrete grade. This is caused by the tube deformation pattern, that is buckling, during which the tube wall experiences local bending along the circumference. During single-axis bending, providing the same curvature of the neutral axis, the larger is the structural element thickness, the higher is its strain along the neutral axis. Hence, for a thick tube, the ultimate strain is accumulated earlier during its buckling than for a thinner tube.

As it can be seen in Fig. 17, in the cases when the vertical load acts onto both the steel tube and the concrete core, the ultimate load values for both limit states of the first group vary almost linearly with the tube thickness for all the considered concrete grades. This linear dependence also takes place in the case of the tubular steel column, depicted in Fig. 17 as well.

It follows from Figs. 18 and 19, that the steel tube confinement increases the column strength, characterized by the first limit state of the first group, several times compared to that of the column made of plain concrete and having the same diameter, as the diameter of the concrete core. Moreover, in the cases, when the steel tube acts only as a confinement (and the vertical load acts only onto the concrete core), its effect onto the steel tube confined concrete column strength is even greater than in the cases, when the vertical load acts onto the ends of both the steel tube and the concrete core. The explanation is simple. The steel tube is barreling under compression, that decreases its confining effect.

From Fig. 20, it is clear that the steel tube confined concrete column strength, associated with the first limit state of the first group, varies almost linearly with the tube thickness for both considered structural schemes of the column, and for all the considered concrete grades, as has been already partially discussed above.

6. CONCLUSION

In the present work, the axially compressed circular steel tube confined concrete columns have been parametrically analyzed through numerical simulation. Several reference cases with the plain concrete circular columns and the tubular steel columns have also been simulated. Totally, 33 different cases have been considered. The general aim has been to confirm the effectiveness of concrete confinement and quantitatively estimate it.

To perform the parametrical analysis, two limit states of the first group, characterized by values of the vertical displacement of the column end and the vertical load, have been defined for the considered cases. The first limit state of the first group has been associated with either concrete failure throughout some cross-section along the column or, for tubular steel columns, transition of some cross-section along the column into the plastic phase throughout its area. The second limit state of the first group has been associated with failure of the steel tube (in the relevant cases) at some circumferential cross-section along the column.

The first group of column limit states and corresponding column failure mechanisms have been investigated, qualitatively and quantitatively, with regard to their dependence onto column structural scheme (viz. whether the vertical load acts onto the end of both the concrete core and the steel tube or only the concrete core is subjected to axial loading, while the steel tube acts only as a confinement), steel tube thickness and concrete grade.

The effectiveness of concrete confinement has been clearly confirmed.

It has been revealed that the steel tube confined concrete column strength, associated with the first limit state of the first group, varies almost linearly with the tube thickness for both considered structural schemes of the column, and for all the considered concrete grades. The largest value of the column strength increase factor k (defined as the ratio of the steel tube confined concrete column strength to the strength of the column made of plain concrete with the diameter equal to that of the concrete core of the steel tube confined concrete column) amounts to 9.36 and has been calculated for the B30 grade concrete and the structural scheme of the column,

in which the steel tube with the thickness of 30 mm acts only as a confinement.

It has also appeared that, when the steel tube acts only as a confinement and the vertical load acts only onto the concrete core, the steel tube confining effect is stronger and the column strength is higher than in the case, when the vertical load acts onto the end of both the concrete core and the steel tube.

Finally, it has been shown that it is ineffective to utilize concrete grades above B60, since the high-strength concrete is more brittle.

Speculating onto directions for future research, one may propose to extend the present one onto eccentric compression and other shapes of the column cross-section. Various techniques of steel confinement anchorage into the concrete core also seems to be a prospective area of research.

7. ACKNOWLEDGEMENT

The research was funded by the National Research Moscow State University of Civil Engineering.

REFERENCES

1. SP 63.13330.2018. Concrete and reinforced concrete structures. General provisions / Russian Building Codes and Regulations 52-01-2003. – With Revs. 1, 2. – Moscow, Russia: Standartinform, 2018, 2020; Russian Standardization Institute, 2022. – VI, 143 p., 21 p., 12 p. : illust.
2. **Lubliner, J., Oliver, J., Oller, S., Oñate, E.** A plastic-damage model for concrete // Int. J. Solids Struct. – 1989. – Vol. 25. – Iss. 3. – P. 229-326.
3. **Argyris, J.H., Faust, G., Szimmat, J., Warnke, E.P., Willam, K.J**. Recent developments in the finite element analysis of prestressed concrete reactor vessels // Nucl. Engng. Design. – 1974. – Vol. 28. – Iss. 1. – P. 42-75.
4. **Willam, K.J., Warnke, E.P.** Constitutive model for the triaxial behavior of concrete / In: IABSE reports. Volume 19. Proceedings of the Seminar on Concrete Structures Subjected to Triaxial Stresses, Bergamo, Italy, 1974. – Zurich, Switzerland: IABSE, 1975. – P. 1-30.
5. **Ottosen, N.S.** A failure criterion for concrete // J. Engng. Mech. Div., Proc. ASCE. – 1977. – Vol. 103. – Iss. EM4. – P. 527-535.
6. **Hsieh, S.S., Ting, E.C., Chen, W.F.** An elastic-fracture model for concrete / In: Proceedings of the 3rd ASCE-EMD Specialty Conference on Mechanics in Engineering, Austin, TX, USA, 1979. – [New York, NY, USA]: [ASCE], 1979. – P. 437-441.
7. Abaqus Analysis User's Manual / Providence, RI, USA: Dassault Systèmes Simulia Corp., 2025.
8. Abaqus Theory Manual / Providence, RI, USA: Dassault Systèmes Simulia Corp., 2025.
9. **Nowacki, W.** The theory of elasticity (in Russian) / Transl. from Pol. by B.E. Pobedrya. – Moscow, USSR: Mir, 1975. – 872 p.
10. **Timoshenko, S.P.** History of strength of materials. With a brief account of the history of theory of elasticity and theory of structures / New York, NY, USA: McGraw-Hill Book Company, 1953. – 452 p.
11. **Von Mises, R.** Mechanik der festen Körper im plastisch deformablen Zustand // Nachr. Ges. Wiss. Göttingen. Math.-Phys. – 1913. – Vol. 1. – P. 582-592.
12. **Khan, A.S., Huang, S.** Continuum theory of plasticity / New York, NY, USA: John Wiley & Sons, 1995. – 431 p.
13. **Mariotte, M.** Traité du mouvement des eaux et des autres corps fluides / Divisé en cinq parties, par feu M. Mariotte de l'Académie Royale des Sciences, mis en lumière par les soins de M. de la Hire, lecteur et professeur du Roy pour les mathématiques et de l'Académie Royale des Sciences. – Paris, France: E. Michallet, 1686.

14. SP 16.13330.2017. Steel structures / Russian Building Codes and Regulations II-23-81*. – With Revs. 1, 2, 3, 4, 5, 6. – Moscow, Russia: Standartinform, 2017, 2019, 2020; Russian Standardization Institute, 2022, 2022, 2023, 2025. – V, 140 p., 8 p., 17 p., 18 p., 2 p., 6 p., 13 p. : illust.
15. **Lee, J., Fenves, G.L.** Plastic-damage model for cyclic loading of concrete structures // J. Eng. Mech. – 1998. – Vol. 124. – Iss. 8. – P. 892-900.
16. **Duvaut, G., Lions, J.L.** Les inéquations en Mécanique et en Physique / Paris, France: Dunod, 1972. – XX, 387 p.

СПИСОК ЛИТЕРАТУРЫ

1. СП 63.13330.2018 «СНиП 52-01-2003. Бетонные и железобетонные конструкции. Основные положения» : Свод правил : Изд. офиц. : Утв. … " " 2019 г. ; с Изм. 1, 2, утв. … " " 2020 г., 2022 г. / Министерство строительства и жилищно-коммунального хозяйства Российской Федерации (Минстрой РФ). – М.: Стандартинформ, 2018, 2020; Российский институт стандартизации, 2022. – VI, 143 с., 21 с., 12 с. : ил.
2. **Lubliner, J., Oliver, J., Oller, S., Oñate, E.** A plastic-damage model for concrete // Int. J. Solids Struct. – 1989. – Vol. 25. – Iss. 3. – P. 229-326.
3. **Argyris, J.H., Faust, G., Szimmat, J., Warnke, E.P., Willam, K.J.** Recent developments in the finite element analysis of prestressed concrete reactor vessels // Nucl. Engng. Design. – 1974. – Vol. 28. – Iss. 1. – P. 42-75.
4. **Willam, K.J., Warnke, E.P.** Constitutive model for the triaxial behavior of concrete / In: IABSE reports. Volume 19. Proceedings of the Seminar on Concrete Structures Subjected to Triaxial Stresses, Bergamo, Italy, 1974. – Zurich, Switzerland: IABSE, 1975. – P. 1-30.
5. **Ottosen, N.S.** A failure criterion for concrete // J. Engng. Mech. Div., Proc. ASCE. – 1977. – Vol. 103. – Iss. EM4. – P. 527-535.
6. **Hsieh, S.S., Ting, E.C., Chen, W.F.** An elastic-fracture model for concrete / In: Proceedings of the 3rd ASCE-EMD Specialty Conference on Mechanics in Engineering, Austin, TX, USA, 1979. – [New York, NY, USA]: [ASCE], 1979. – P. 437-441.
7. Abaqus Analysis User's Manual / Providence, RI, USA: Dassault Systèmes Simulia Corp., 2025.
8. Abaqus Theory Manual / Providence, RI, USA: Dassault Systèmes Simulia Corp., 2025.
9. **Новацкий, В.** Теория упругости / Пер. с пол. Б.Е. Победри. – М.: Мир, 1975. – 872 с.
10. **Timoshenko, S.P**. History of strength of materials. With a brief account of the history of theory of elasticity and theory of structures / New York, NY, USA: McGraw-Hill Book Company, 1953. – 452 p.
11. **Von Mises, R.** Mechanik der festen Körper im plastisch deformablen Zustand // Nachr. Ges. Wiss. Göttingen. Math.-Phys. – 1913. – Vol. 1. – P. 582-592.
12. **Khan, A.S., Huang, S.** Continuum theory of plasticity / New York, NY, USA: John Wiley & Sons, 1995. – 431 p.
13. **Mariotte, M**. Traité du mouvement des eaux et des autres corps fluides / Divisé en cinq parties, par feu M. Mariotte de l'Académie Royale des Sciences, mis en lumière par les soins de M. de la Hire, lecteur et professeur du Roy pour les mathématiques et de l'Académie Royale des Sciences. – Paris, France: E. Michallet, 1686.
14. СП 16.13330.2017 «СНиП II-23-81*. Стальные конструкции» : Свод правил : Изд. офиц. : Утв. … " " 2017 г. ; с Изм. 1, 2, 3, 4, 5, 6, утв. … " " 2019 г., 2020 г., 2022 г., 2022 г, 2023 г, 2025 г. / Министерство строительства и жилищно-коммунального хозяйства Российской Федерации (Минстрой РФ). – М.: Стандартинформ, 2017, 2019, 2020; Российский институт

стандартизации, 2022, 2022, 2023, 2025. – V, 140 с., 8 с., 17 с., 18 с., 2 с., 6 с., 13 с. : ил.
15. **Lee, J., Fenves, G.L.** Plastic-damage model for cyclic loading of concrete structures // J. Eng. Mech. – 1998. – Vol. 124. – Iss. 8. – P. 892-900.
16. **Duvaut, G., Lions, J.L.** Les inéquations en Mécanique et en Physique / Paris, France: Dunod, 1972. – XX, 387 p.

Vladislav Vladimirovich Vershinin – senior lecturer at the Department of Structural Metal and Timber, National Research Moscow State University of Civil Engineering (NRU MGSU), 26 Yaroslavskoe shosse, Moscow, 129337, Russia; vlodya_91@mail.ru; +79165225509.

Владислав Владимирович Вершинин – старший преподаватель кафедры Металлических и деревянных конструкций, Национальный исследовательский Московский государственный строительный университет (НИУ МГСУ), д. 26, Ярославское шоссе, г. Москва, 129337, Россия; vlodya_91@mail.ru